Momentum theory of Joukowsky actuator discs with swirl

Gijs A. M. van Kuik
Duwind, Delft University of Technology, Kluyverweg 1, 2629HS Delft, NL
E-mail: g.a.m.vankuik@tudelft.nl

Abstract. Actuator disc theory is the basis for most rotor design methods, be it with many extensions and engineering rules added to make it a well-established method. However, the off-design condition of a very low rotational speed Ω of the disc is still a topic for scientific discussions. Several authors have presented solutions of the associated momentum theory for actuator discs with a constant circulation, the so-called Joukowsky discs, showing the efficiency $C_p \rightarrow \infty$ for $\Omega \rightarrow 0$. The momentum balance is very sensitive to the choice of the vortex core radius δ as the pressure and velocity gradients become infinite for $\delta \rightarrow 0$. Viscous vortex cores do not show this singular behaviour so an inviscid core model is sought which removes the momentum balance sensitivity to singular flow. A vortex core with a constant δ does so. Applying this results in $C_p \rightarrow 0$ for $\Omega \rightarrow 0$, instead of $C_p \rightarrow \infty$. The Joukowsky actuator disc theory is confirmed by a very good match with the numerically obtained results. It gives higher C_p values than corresponding solutions for discs with a Goldstein-based wake circulation published in literature.

1. Introduction

Although the concept of the actuator disc is more than 100 years old, it is still the basis for rotor design codes using the blade element momentum theory developed over these 100 years, see [1]. In recent years the behaviour of actuator disc flows with a low rotational speed has been studied by several authors, providing several solutions depending on the type of load that is applied, see e.g. [2]. Research has focussed on rotors and discs having a constant circulation in the wake, known as the Joukowsky distribution [3], or the Betz distribution [4] yielding a helicoidal wake structure moving with a uniform axial velocity. Goldstein [5] was the first to find a solution for this wake for lightly loaded propellers, see [6] for an overview. Both distributions were assumed to represent the circulation distribution of an ideal rotor. The present paper considers the Joukowsky distribution and compares the results with solutions of the Betz-Goldstein distribution modified for heavily loaded actuator discs reported in [7, 8] and [9].

The swirl of the wake is induced by a discrete vortex at the wake centre line, leading to an infinite azimuthal velocity and pressure for the radius $r \rightarrow 0$. The question how to model the discrete vortex and how this impacts the momentum balance has been studied by e.g. [10, 11, 12, 13, 14]. All performance predictions reported in these references show a remarkable result: in the limit to zero rotational speed the efficiency of the disc increases to infinity, which is highly non-physical.

Within the inviscid flow regime, the analysis in [14] is considered to be exact apart from the choice of the vortex core at the axis of the wake. The centreline vortex is a Rankine vortex of which the core diameter is proportional to the wake radius. The analysis shows that adding a disturbance parameter to the momentum balance removes the non-physical result of infinite efficiency for zero rotational speed, no matter how small this disturbance is. This is an indication that the momentum balance is very sensitive to small deviations in the flow parameters.

A failed attempt to reproduce the results of [14] by the potential flow actuator disc code described in [15] initiated a re-analysis of the vortex core model and its impact on the momentum theory. In section 2 the equations of motion for Joukowsky actuator disc flows are given as well as for the disc loading and far wake properties. Herewith the general mass, momentum and energy balances are derived in section 3.1, followed by section 3.2 where the vortex core model is analysed. The chosen core model is applied in section 3.3. Section 4 describes the numerical approach, after which the results of the calculations and momentum theory are compared in section 5.

2. The equations of motion

2.1. The equations for a disc with constant circulation

The flow is governed by the Euler equation:

$$\frac{1}{\rho}\left(\boldsymbol{f}-\boldsymbol{\nabla}p\right)=\boldsymbol{v}\cdot\boldsymbol{\nabla}\boldsymbol{v} \tag{1}$$

in which ρ is the fluid density [kg/m^3], f the force density [N/m^3], p the static pressure [N/m^2], $\boldsymbol{v}$ the velocity vector [m/s] and $H=p+\frac{1}{2}\rho\boldsymbol{v}\cdot\boldsymbol{v}$ the total pressure [N/m^2]. Also the equivalent formulation:

$$\boldsymbol{f}=\boldsymbol{\nabla}H-\rho\boldsymbol{v}\times\boldsymbol{\omega} \tag{2}$$

will be used. A cylindrical reference system (x,r,φ) is applied, with the positive x coinciding with the downwind wake axis, and with r and φ the radial and azimuthal coordinate, see figure 1. For the special case of a disc flow with constant circulation induced by a free vortex Γ at the axis of the wake the azimuthal velocity in the wake is:

$$\Gamma=2\pi r v_\varphi. \tag{3}$$

The vortex is a potential flow vortex, with a vortex core having diameter $\delta(x)$. It is common to model the core as a Rankine vortex, characterized by solid body rotation of the flow, after which the limit of $\delta\to 0$ is taken. Figure 1 shows (half of) the cross section through the stream-tube in the meridian plane, with the disc and fully developed wake indicated. The disc has radius R and area A, while A_1 is the area of the far wake with radius R_1. In the remainder the index 0 is used for flow variables in the undisturbed, upstream flow. The fully developed far wake is indicated by the index 1, see figure 1. If there is no index, the variables are taken at the position of the actuator disc.

2.2. The disc load

Only the pressure and the azimuthal velocity will be discontinuous across the infinitesimal thin disc, so integration of the axial and azimuthal component of (1) gives:

$$\frac{1}{\rho}\boldsymbol{F}=\boldsymbol{e}_x\frac{\Delta p}{\rho}+\boldsymbol{e}_\varphi v_x\Delta v_\varphi \tag{4}$$

$$=\boldsymbol{e}_x\Delta\left(\frac{H}{\rho}-\frac{1}{2}v_\varphi^2\right)+\boldsymbol{e}_\varphi v_x\Delta v_\varphi \tag{5}$$

where F denotes a surface load [N/m^2], Δ the difference between the down- and upwind side of the disc and $\boldsymbol{e}$ the unit vector. As $v_\varphi = 0$ at the upwind side of the disc $\Delta v_\varphi = v_\varphi$. In (5) the Bernoulli equation integrated across the disc thickness has been used:

$$\Delta p = \Delta H - \frac{1}{2}\rho v_\varphi^2. \tag{6}$$

The local power converted by the force field $\boldsymbol{f}$ is $\boldsymbol{f} \cdot \boldsymbol{v}$ which has to be equal to the local contribution to the torque, $r f_\varphi$, times rotational speed Ω. The converted power $\boldsymbol{f} \cdot \boldsymbol{v}$ becomes:

$$\boldsymbol{f} \cdot \boldsymbol{v} = \Omega r f_\varphi = (\boldsymbol{v} \cdot \boldsymbol{\nabla})\, H. \tag{7}$$

This shows that the work done by the force field is expressed in a change in the total pressure or Bernoulli constant H. Integration of (7) across the thickness combined with the azimuthal component of (4) gives the general expression:

$$\Delta H = \frac{\Omega r}{v_x} F_\varphi = \rho \Omega r v_\varphi \tag{8}$$

and, with (3), for the Joukowsky disc:

$$\frac{1}{\rho}\Delta H = \frac{\Omega \Gamma}{2\pi}. \tag{9}$$

The sign conventions are that the rotational speed $\Omega > 0$ and $\Gamma < 0$ so $\Delta H < 0$ implying that energy is extracted from the flow.

2.3. The far wake

With the conservation of circulation:

$$r v_\varphi = r_1 v_{\varphi,1} \tag{10}$$

the Bernoulli equation (9) is written as:

$$\frac{1}{\rho}\left(p_0 - p_1\right) = \frac{1}{2}\left(v_{x,1}^2 - U_0^2 + v_{\varphi,1}^2\right) - \frac{\Omega \Gamma}{2\pi}. \tag{11}$$

Differentiating with respect to r and combining it with the radial pressure equilibrium in the far wake:

$$\frac{\partial p_1}{\partial r_1} = \rho \frac{v_{\varphi,1}^2}{r_1} \tag{12}$$

it is clear that $v_{x,1}$ is constant. By this (11) can be written as:

$$p_1 - p_0 = -\frac{1}{2}\rho v_{\varphi,1}^2 + p^*. \tag{13}$$

At the wake boundary the pressure has to be undisturbed (p_0), so $p^* = \frac{1}{2}\rho v_{\varphi,R_1}^2$ and, with (3):

$$p_1 - p_0 = -\frac{1}{2}\rho v_{\varphi,1}^2 + \frac{1}{2}\rho \left(\frac{\Gamma}{2\pi R_1}\right)^2 \tag{14}$$

or:

$$\frac{p_1 - p_0}{\rho} = \frac{1}{2}\left(v_{\varphi,R_1}^2 - v_{\varphi,1}^2\right) = \frac{1}{2}\left[\left(\frac{\Gamma}{2\pi R_1}\right)^2 - \left(\frac{\Gamma}{2\pi r_1}\right)^2\right]. \tag{15}$$

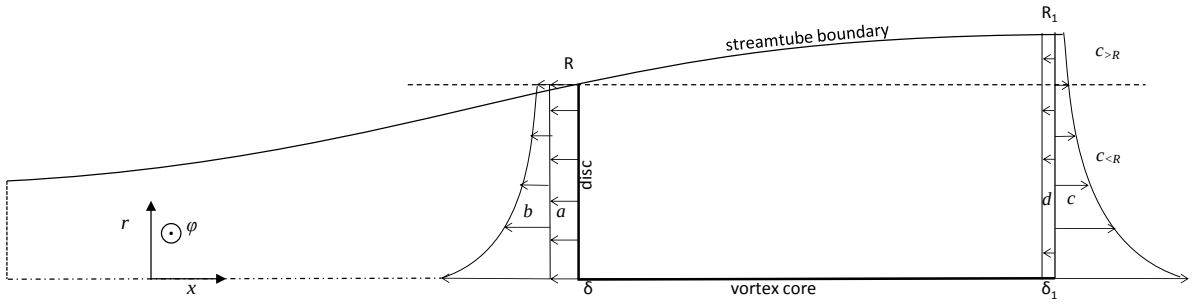

Figure 1. Pressure distributions acting in the momentum balance. The meaning of a, b, c and d is given in the main text.

3. Momentum theory

3.1. The momentum, mass and energy balance

The momentum equation drawn on the stream-tube as control volume, see figure 1, is written as:

$$T - \int_{A_1} (p_1 - p_0)\, dA_1 = \rho \int_{A_1} v_{x,1}\,(v_{x,1} - U_0)\, dA_1 \tag{16}$$

where T is the thrust [N] being the integrated pressure jump across the disc. It is convenient to split A and A_1 in two parts: the area inside the vortex core, so $r < \delta$ or δ_1, and outside of it $\delta < r < R$ or $\delta_1 < r_1 < R_1$. Irrespective of the choice for δ/δ_1, in the limit $\delta \to 0$ the core area only contributes to the momentum balance when the pressure or momentum flux is of order $O(\delta^2)$ or higher. In [14] this is analysed for the Rankine root vortex, showing that this is not the case. The same holds for the energy balance. Consequently in the remainder of the present analysis the flow region $r < \delta$ or δ_1 is discarded, with an exception for section 3.2.

Figure 1 shows the pressure distributions appearing in the left hand side of (16) including the thrust:

a) constant pressure jump across the disc giving the jump in Bernoulli parameter H according to the first term at the right hand side of (6).
b) pressure distribution due to jump in v_φ according to the second term at the right hand side of (6).
c) the same pressure distribution in the far wake due to the v_φ distribution according to the first term at the right hand side of (14).
d) constant pressure to achieve $p_1 - p_0 = 0$ according to the second term at the right hand side of (14).

When these contributions are expressed in Γ by (3) and (8), integrated, subjected to $\lim \delta \to 0$, substituted in (16) and divided by the disc surface πR^2 the result is:

$$\frac{\Omega\Gamma}{2\pi} - \frac{1}{2}\left(\frac{\Gamma}{2\pi R}\right)^2 - \left(\frac{\Gamma}{2\pi R}\right)^2 \left[\int_\delta^R \frac{dr}{r} - \int_{\delta_1}^{R_1} \frac{dr_1}{r_1}\right] = v_{x,1}\,(v_{x,1} - U_0)\left(\frac{R_1}{R}\right)^2 \tag{17}$$

where the left hand side terms give the contribution of a, d, b and c. The mass balance is:

$$\frac{\overline{v_x}}{v_{x,1}} = \left(\frac{R_1}{R}\right)^2 \tag{18}$$

with the bar above v_x indicating that it is the average value. The energy balance follows from the combination of (11) and (15):

$$\frac{\Omega\Gamma}{2\pi} - \frac{1}{2}\left(\frac{\Gamma}{2\pi R_1}\right)^2 = \frac{1}{2}\left(v_{x,1}^2 - U_0^2\right). \tag{19}$$

Mixing (17) and (18) simplifies the right hand side of the momentum balance yielding:

$$\frac{\Omega\Gamma}{2\pi} - \frac{1}{2}\left(\frac{\Gamma}{2\pi R}\right)^2 - \left(\frac{\Gamma}{2\pi R}\right)^2 \left[\int_\delta^R \frac{dr}{r} - \int_{\delta_1}^{R_1} \frac{dr_1}{r_1}\right] = \overline{v_x}\left(v_{x,1} - U_0\right). \tag{20}$$

The non-dimensional tip speed ration $\lambda = \frac{\Omega R}{U_o}$, and non-dimensional vortex $q = \frac{-\Gamma}{2\pi R U_o}$ are introduced. As $\Gamma < 0$ $q > 0$. Furthermore from here on $\overline{v_x}$ and $v_{x,1}$ indicate the dimensionless value $\frac{\overline{v_x}}{U_0}$ respectively $\frac{v_{x,1}}{U_0}$. Herewith (9) becomes:

$$\frac{1}{\rho}\frac{\Delta H}{U_0^2} = -\lambda q, \tag{21}$$

and the momentum balance:

$$2\lambda q + q^2 + 2q^2\left[\ln\frac{R}{\delta} - \ln\frac{R_1}{\delta_1}\right] = 2\overline{v_x}\left(1 - v_{x,1}\right) \tag{22}$$

as well as the energy balance:

$$2\lambda q + q^2\left(\frac{R}{R_1}\right)^2 = \left(1 - v_{x,1}^2\right). \tag{23}$$

These equations can be solved for $\overline{v_x}$ once the term within the square brackets is known or more precisely: when the vortex core development is known. When $\overline{v_x}$ is known the power coefficient $C_p = P/(\frac{1}{2}\rho U_0^3 \pi R^2)$ follows by integration of (7) on the disc area:

$$C_p = 2\lambda q \overline{v_x}. \tag{24}$$

The thrust coefficient $C_T = T/(\frac{1}{2}\rho U_0^2 \pi R^2)$ contains the contributions a and b shown in figure 1, here denoted as ΔH respectively $\Delta\varphi$:

$$C_T = C_{T,\Delta H} + C_{T,\Delta\varphi} = 2\lambda q + q^2 \ln\left(\frac{R}{\delta}\right)^2. \tag{25}$$

3.2. The choice of the vortex core model

The momentum theory results are very sensitive to the choice of δ and δ_1 because of the logarithmic singularity in (22) for $\delta, \delta_1 \to 0$. In [14] it is assumed that the core diameter scales with the radius of the wake because of mass conservation, so $\delta/R = \delta_1/R_1$. The two terms within the square brackets of (22) cancel each other so only pressure distributions a and d appear in the momentum balance. This holds for $\delta \to 0$ as well as for $\delta \neq 0$. However, this choice assumes that $\overline{v_{x,core}} = \overline{v_x}$, which is is not correct. The distribution $v_x(r)$ is known from calculations like in [15] showing that for small r $v_x > \overline{v_x}$. As the velocity at both sides of the core radius are equal, $v_{x,core} > \overline{v_x}$ which invalidates the assumption $\delta/R = \delta_1/R_1$.

Because of the singular flow behaviour for $\delta \to 0$, it is questionable whether the Euler flow equations are able to represent this flow with infinite pressure and velocity gradients, as it is not

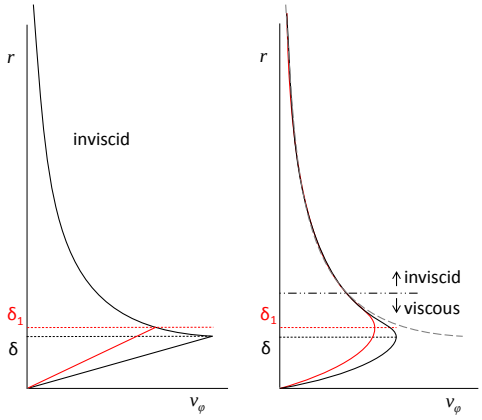

Figure 2. Qualitative sketch of the inviscid distribution of v_φ and the partly inviscid, partly viscous distribution.

a priori clear whether viscous effects may be ignored. Therefore the question is posed: *which inviscid core model represents best the behaviour of a viscous vortex core?*

To allow for other distributions of v_φ than (3) plus the Rankine vortex core, first the third term at the left hand side of (20) is reformulated in terms of v_φ:

$$-\frac{1}{R^2}\left[\int_0^R v_\varphi^2 r dr - \int_0^{R_1} v_{\varphi,1}^2 r dr\right] = \frac{1}{R^2}\left[\int_R^{R_1} v_{\varphi,1}^2 r dr - \int_0^R \left(v_\varphi^2 - v_{\varphi,1}^2\right) r dr\right] \tag{26}$$

with the lower bound of the integrals set to 0. In [16] the development of a viscous vortex core is treated. Diffusion and stretching-compression of vorticity modify the potential flow behaviour. For a specific accelerating vortex flow, the Burgers vortex, the diffusion and stretching counteract in such a way that the distribution of $v_\varphi(r)$ is invariant, see [16], so $v_\varphi = v_{\varphi 1}$. For a decelerating vortex such a solution is not known. The vortex is compressed giving a similar vorticity spreading effect as diffusion. Figure 2.8 in [16] shows the development over time of v_φ due to diffusion. Asuming that time may be replaced by downstream distance divided by velocity, figure 2 shows qualitatively the development of v_φ from disc to wake, both for inviscid and viscous flows. The viscous distribution does not show a singular behaviour. As it is not known what $v_{\varphi,\max}/v_{\varphi 1,\max}$ and δ/δ_1 are, the difference-integral in (26) cannot be evaluated without detailed calculations. However, as viscosity keeps the pressure and v_φ limited the second integral in the right hand side of (26) will not not contribute when $\delta, \delta_1 \ll R, R_1$. Then the first integral remains so, in dimensionless form:

$$-\frac{1}{R^2}\left[\int_0^R v_\varphi^2 r dr - \int_0^{R_1} v_{\varphi,1}^2 r dr\right] = q^2 \ln\frac{R}{R_1}. \tag{27}$$

The same result is obtained in the inviscid model of a potential vortex plus Rankine vortex core by assuming $\delta = \delta_1$, as is clear by (22). This model has the drawback that the flow inside a decelerating core with constant but non-zero δ does not satisfy the continuity equation. However, this drawback is removed for $\delta \to 0$. Consequently *an inviscid core with an infinitely small but constant radius* represents best the behaviour of a viscous vortex core. This model will be applied in the next section.

3.3. The JMT:Joukowsky actuator disc momentum theory with swirl
With $\delta = \delta_1 \to 0$ contribution b is cancelled by $c_{<R}$ which is the part of c up to $r_1 = R$. Now the pressure fields a, $c_{>R}$ and d appear in the momentum balance. With the term with square bracket in (22) becomes:

$$-2q^2 \ln\left(\frac{R_1}{R}\right) = -q^2 \ln\left(\frac{R_1}{R}\right)^2 \tag{28}$$

and the momentum balance, making use of (18):

$$2\lambda q + q^2\left(1 - \ln\left(\frac{\overline{v_x}}{v_{x,1}}\right)\right) = 2\overline{v_x}\left(1 - v_{x,1}\right). \tag{29}$$

The energy balance (23) is unchanged.

By mixing (23) and (29) the velocity at the disc can be written as:

$$\overline{v_x} = \frac{1}{2}\left(v_{x,1}+1\right)\frac{\lambda q + \frac{1}{2}q^2\left(1 + \ln\left(\frac{R}{R_1}\right)^2\right)}{\lambda q + \frac{1}{2}q^2\left(\frac{R}{R_1}\right)^2}. \tag{30}$$

As $\left(1 + \ln\left(R/R_1\right)^2\right) < \left(R_1/R\right)^2$ for $R < R_1$ the ratio is < 1. Consequently $\overline{v_x} < 0.5\left(v_{x,1}+1\right)$. The ratio in (30) is the ratio between the left hand side of the momentum balance (22) and energy balance (23) or, in other words, between the total load exerted on the flow in the stream-tube control volume and the non-conservative load which is the load performing work. By this, (30) is equivalent to equation 6 of [15], where the distinction between the conservative and non-conservative loads is used to explain the results of the momentum theory applied to an annulus of the stream-tube.

An analytical solution of (23) and (29) is not found. An implicit expression of $v_{x,1}$ in the independent variables λ, q is obtained by writing (23) as an expression for $\overline{v_x}$ with the help of (18) and substitute this in (29):

$$\frac{\left(1 - v_{x,1}\right)v_{x,1}q^2}{1 + 2\lambda q - v_{x,1}^2} = \left(q\lambda - \frac{1}{2}q^2\left(1 - \ln\left(\frac{q^2}{1 + 2\lambda q - v_{x,1}^2}\right)\right)\right). \tag{31}$$

This can be solved numerically for $v_{x,1}$. The wake expansion follows by (23) and the velocity at the disc by (29). Finally C_p is given by (24).

3.4. JMT limit values for $\lambda \to 0$ and $\lambda \to \infty$
For large values of λ the wake angular momentum should go to 0, and the momentum theory should become the one-dimensional theory yielding the well-known Betz-Joukowsky maximum value for C_p. According to (21) q is inversely proportional to λ for constant ΔH or λq. In the balances (23) and (29) the q^2 terms vanish for $\lambda \to 0$ with which indeed the momentum theory without wake swirl is recovered.

For the limit $\lambda \to 0$ flow states with $\lambda q = \textit{constant}$ are studied first. The energy balance (23) shows that, provided $R/R_1 \neq 0$, the highest value for q^2 is obtained for $v_{x,1} = 0$, giving:

$$2\lambda q + q^2\left(\frac{R}{R_1}\right)^2 = 1. \tag{32}$$

The right hand side of the momentum balance (29) is 0 for $v_{x,1} = 0$, see (17), by which it becomes, using (18):

$$2\lambda q + q^2\left(1 - \ln\left(\frac{R_1}{R}\right)^2\right) = 0. \tag{33}$$

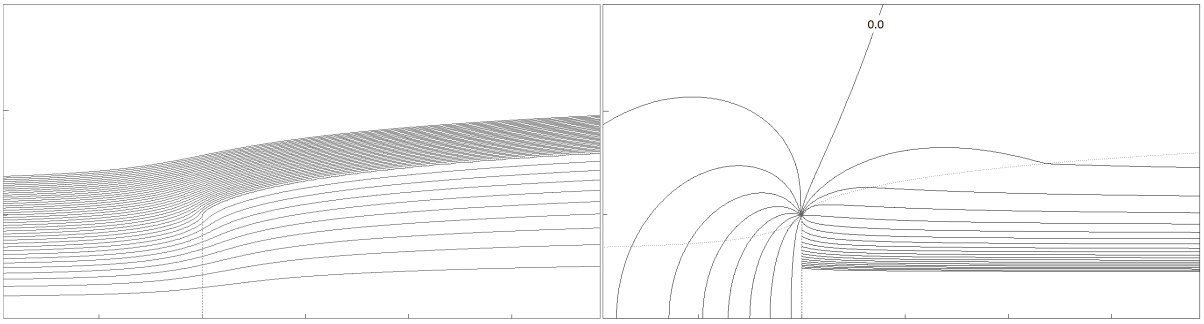

Figure 3. Streamlines with $\Delta\psi = 0.1\Delta\psi_{wake}$ and isobars with $\Delta p = 0.1\Delta H$ for $\Delta H/(\frac{1}{2}\rho U_0^2) = -0.8888$ and $\lambda = 0.73$. Ticks at the axes are at a $1R$ interval.

Elimination of q^2 from (32) and (33) gives the wake expansion for the highest q - lowest λ:

$$\left(\frac{R_1}{R}\right)^2 \left(1 - \ln\left(\frac{R_1}{R}\right)^2\right) = \frac{2\lambda q}{2\lambda q - 1}. \tag{34}$$

As an example, $2\lambda q = 8/9$ results in $\frac{R_1}{R} = 2.77$, $q = 0.924$ by (32) and $\lambda = 0.48$. The assumption $R/R_1 \neq 0$ is satisfied, showing that both $\overline{v_x}$ and $v_{x,1}$ are 0, but the ratio of $\frac{\overline{v_x}}{v_{x,1}} \to 7.69$. This flow state is characterized by a full blockage by the disc, creating a wake with azimuthal flow only, so there is no change in axial momentum. The associated pressure distributions in the wake and at the disc balance each other. A lower value of λ is not possible for this value of λq. For $\lambda q = 0$ (34) gives $R/R_1 = 1$, (32) gives $q = 1$, by which $\lambda = 0$ and $C_p = 0$.

$C_{p,max}(\lambda)$ is obtained by optimizing the solutions for fixed λ varying q.

4. Potential flow calculations

The computer code described in [15] has been adapted to include wakes with swirl. Axial and radial velocities are calculated by summation of the induction by each of the several thousand vortex rings which constitute the wake boundary. The azimuthal velocities are calculated by (3). The shape and strength of the vortex rings are adapted in the convergence scheme to satisfy the two boundary conditions: zero pressure jump across the wake boundary, and zero cross flow. The first boundary condition $\Delta p_{wake-boundary} = 0$ is expressed in $|\boldsymbol{v}|$ and input parameter ΔH: $\Delta(\frac{1}{2}\rho\,|\boldsymbol{v}|^2) - \Delta H = 0$. In [15] $\boldsymbol{v}$ only had an axial and radial component, now the azimuthal component enters the boundary condition. The strength of the vortex at the axis follows from (21) expressed in H and the second input parameter λ: $q = -\Delta H/(\rho U_0^2 \lambda)$. Apart from these changes the code is unmodified. The results satisfy the same accuracy requirements as described in [15]. Figure 3 shows the streamlines, expressed in the stream-function Ψ, and isobars of the disc flow with $\Delta H/(\frac{1}{2}\rho U_0^2) = -0.8888$ and $\lambda = 0.73$. The pressure at the upstream side of the disc is constant, confirming one of the conclusions in [15] that the velocity in the meridian plane, $\{v_x, v_r\}$, is constant. The isobars in the wake show the pressure gradient due to the swirl.

5. Results

Figure 4 shows the comparison of the JMT and the potential flow results. The marker indicating the lowest C_p for $\Delta H/(\frac{1}{2}\rho U_0^2) = -0.8888$ corresponds to the flow in figure 3. The correspondence between the JMT and Potential Flow calculations is excellent. A comparison with the $C_{p,max} - \lambda$ curve for rotors with an infinite number of blades having a modified Betz-Goldstein distribution of the circulation is shown in figure 5. As shown by [7, 8] the original Betz-Goldstein solution

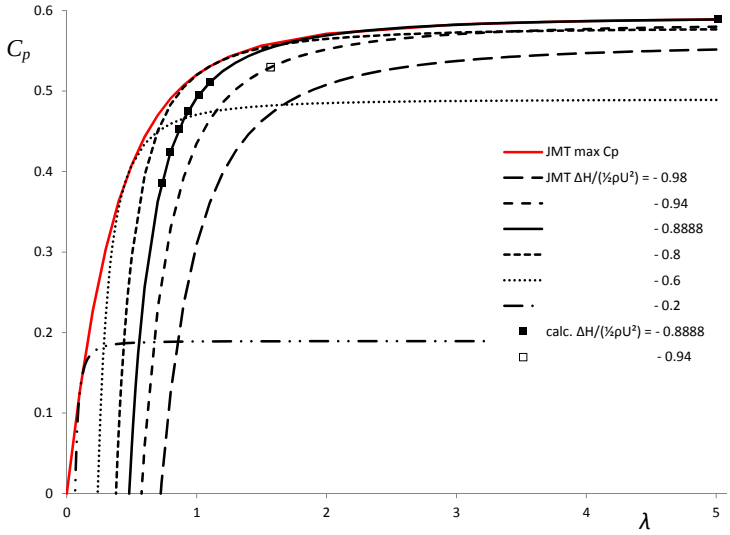

Figure 4. The Joukowsky momentum theory results compared with potential flow calculations.

resulted in $C_{p,max} = 1$, as the pitch of the helicoidal wake was based on the undisturbed velocity. With the pitch based on the velocity in the rotor plane, [8] showed that $C_{p,max}$ reaches the well known Betz-Joukowsky maximum 16/27 for high λ. The $C_{p,max} - \lambda$ curve of this corrected solution expanded to a rotor with an infinite number of blades is shown in figure 3 of [8]. An alternative solution is published in [9] where the Goldstein formulation is adapted to allow for non-zero torque when $\lambda \to 0$. A comparison of the Joukowsky momentum theory and the Betz-Goldstein-Okulov/Wood curves is given in figure 5. The Joukowsky distribution gives higher $C_{p,max}$ than the Betz-Goldstein based distributions, with the difference vanishing for higher λ. This is confirmed by [17] where rotors with a finite number of blades having a Joukowsky and Betz-Goldstein based distribution have been compared.

6. Conclusions

- An actuator disc momentum theory including wake swirl has been developed resulting in the physically plausible result that $C_p \to 0$ in the limit $\lambda \to 0$. For high λ the theory reproduces the results of the classical momentum theory without swirl.
- The novelty in the method is the removal from the momentum balance of the singular behaviour of the pressure near the wake centreline vortex, giving rise to non-physical results in several previously published methods.
- This removal is done by applying a vortex core with constant diameter δ. Support for this is found in the absence of singular flow when viscous core development is considered.
- The momentum theory results are very accurately confirmed by potential flow field calculations.
- The Joukowsky momentum theory results are higher than the equivalent results for rotors with an infinite number of blades optimized for modified Betz-Goldstein solutions.

Acknowledgments

Thanks go to Jens Norkær Sørensen, DTU, for the discussions about the modified momentum theory and the suggestion to look at viscous effects in support for the vortex core model, and to Valery Okulov, DTU, and David Wood, University of Calgary, for a discussion on the Betz-Goldstein solution and for providing the data shown in figure 5.

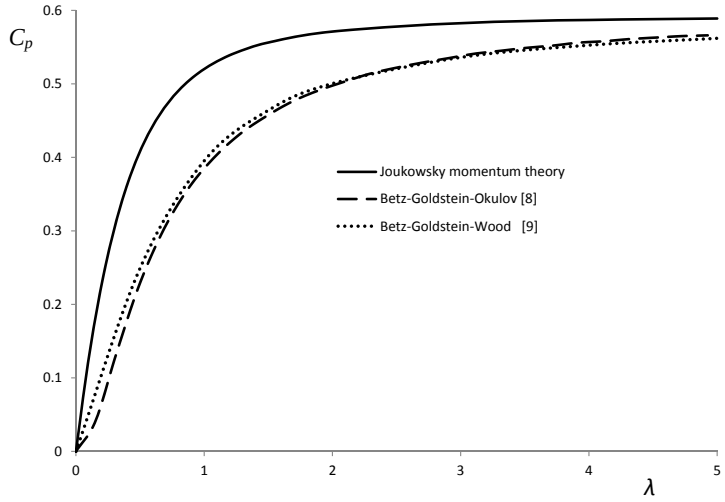

Figure 5. The Joukowsky actuator disc results compared with the Betz-Goldstein solutions of Okulov [8] and Wood [9] for rotors with an infinite number of blades.

References

[1] G. A. M. van Kuik, J. N. Sørensen, and V. L. Okulov. Rotor theories by Professor Joukowsky: Momentum theories. *Progress in Aerospace Sciences*, 73:1–18, 2015.

[2] J. N. Sørensen. *General Momentum Theory for Horizontal Axis Wind Turbines*. Springer International Publishing, Heidelberg, 2015.

[3] J. N. Joukowsky. Vortex theory of the screw propeller IV. *Trudy Avia Raschetno- Ispytatelnogo Byuro 1918;3:197 (in Russian) Also published in Gauthier-Villars et Cie. (eds). Théorie Tourbillonnaire de l'Hélice Propulsive, Quatrième Mémoire. 123146:*, 1918.

[4] A Betz. Schraubenpropeller mit geringstem Energieverlust. *Vier Abhandlungen zur Hydrodynamik und Aerodynamik, Reprint of 4 famous papers by Universitätsverlag Göttingen*, 1927.

[5] S. Goldstein. On the vortex theory of screw propellers. *Proc. R. Soc. Lond. A*, 123:440–465, 1929.

[6] V. L. Okulov, J. N. Sørensen, and D.H. Wood. The rotor theories by Professor Joukowsky: Vortex Theories. *Progress in Aerospace Sciences*, 73:19–46, 2015.

[7] V. L. Okulov and J. N. Sørensen. Refined Betz limit for rotors with a finite number of blades. *Wind Energy*, 11(4):415–426, 2008.

[8] V. L. Okulov. Limit cases for rotor theories with Betz optimization. *Journal of Physics: Conference Series*, 524(Torque2014):012129, 2014.

[9] D. H. Wood. Maximum wind turbine performance at low tip speed ratio. *Journal of Renewable and Sustainable Energy*, 7:053126, 2015.

[10] O. de Vries. *Fluid dynamic aspects of wind energy conversion, AGARDograph 243*. AGARD, Amsterdam, 1979.

[11] D. J. Sharpe. A general momentum theory applied to an energy-extracting actuator disc. *Wind Energy*, 7(3):177–188, jul 2004.

[12] M. I. Xiros and N. I. Xiros. Remarks on wind turbine power absorption increase by including the axial force due to the radial pressure gradient in the general momentum theory. *Wind Energy*, 10(1):99–102, jan 2007.

[13] D. H. Wood. Including swirl in the actuator disk analysis of wind turbines. *Wind Engineering*, 31(5):317–323, 2007.

[14] J. N. Sørensen and G. A. M. van Kuik. General momentum theory for wind turbines at low tip speed ratios. *Wind Energy*, 14:821–839, 2011.

[15] G. A. M. Van Kuik and L. E. M. Lignarolo. Potential flow solutions for energy extracting actuator disc flows. *Wind Energy*, 19:1391–1406, 2016, published online Sept 2015.

[16] S. V. Alekseenko, P. A. Kuibin, and V. L. Okulov. *Theory of Concentrated Vortices*. Springer Verlag, Berlin, Heidelberg, 2007.

[17] V. L. Okulov and J. N. Sørensen. Maximum efficiency of wind turbine rotors using Joukowsky and Betz approaches. *Journal of Fluid Mechanics*, 649:497–508, 2010.